Combined Spectroscopic/ Computational Studies on Fe- and Mn-Dependent Superoxide Dismutases: Insights into Second-Sphere Tuning of Active Site Properties

TIMOTHY A. JACKSON AND
THOMAS C. BRUNOLD*

Department of Chemistry, University of Wisconsin, Madison, Wisconsin 53706

Received February 17, 2004

ABSTRACT

Superoxide dismutases (SODs) are metalloenzymes that protect aerobic organisms from oxidative damage mediated by the superoxide radical. While the Fe- and Mn-dependent SODs from *E. coli* possess virtually identical protein folds and active-site geometries, they are strictly metal specific. To explore the origin of this extraordinary metal-ion specificity and to elucidate the mechanisms by which these enzymes tune the geometric and electronic properties, and thus the reactivity, of their active-site metal ions, we utilized a combination of spectroscopic and computational methods to study the native enzymes, their metal-substituted derivatives, and several mutant proteins. Results from our research described in this Account reveal that second-sphere residues are critically involved in controlling both thermodynamic and kinetic properties of the Fe− and MnSOD active sites.

Introduction

Superoxide dismutases (SODs) are metalloenzymes that defend biological systems against oxidative damage mediated by the superoxide anion ($O_2^{\bullet-}$).[1−4] As all aerobic organisms are susceptible to production of this deleterious radical species during O_2 metabolism (as much as 1−5% of the total O_2 consumed by humans is converted to $O_2^{\bullet-}$),[1,3] Nature has evolved several different SODs that utilize either Fe, Mn, Cu/Zn, or Ni metal cofactors.[3,4] The highly homologous Fe- and Mn-dependent enzymes accomplish their function through disproportionation of $O_2^{\bullet-}$ to O_2 and H_2O_2 (eq 1, where M corresponds to Fe or Mn)[1−3]

$$M^{3+}SOD + O_2^{\bullet-} \rightarrow M^{2+}SOD + O_2 \quad (1a)$$

$$M^{2+}SOD + O_2^{\bullet-} + 2H^+ \rightarrow M^{3+}SOD + H_2O_2 \quad (1b)$$

Fe− and MnSODs consist of dimers or tetramers of subunits of about 21 kDa that share substantial sequence similarity and possess virtually identical protein folds and active-site geometries.[5,6] The metal ion is in a distorted trigonal bipyramidal coordination environment consisting of His26 and a solvent molecule in the axial positions and His73(81), His160(171), and Asp156(167) in the equatorial plane (see Figure 1 for numbering scheme). The solvent ligand, which cycles between the hydroxo and aqua forms depending on the metal oxidation state (eq 2),[3,7] participates in a H-bond network that includes Asp156(167) and the conserved second-sphere residues Gln69(146) and Tyr34.

$$M^{3+}-OH + 1e^- + 1H^+ \leftrightarrow M^{2+}-OH_2 \quad (2)$$

The second-order rate constants for $O_2^{\bullet-}$ disproportionation catalyzed by *E. coli* Fe− and MnSODs approach the diffusion-controlled limit,[1,3] though for the latter enzyme the kinetics are complicated by the occasional formation of a "dead-end" complex described as a side-on peroxo−Mn^{3+} species based on its absorption spectrum.[3] In each case the turnover number exhibits a moderate solvent isotope effect of ∼3, suggesting that proton transfer is involved in the rate-limiting step.[1] Consistent with the requirement for two protons in the catalytic cycle (eq 1), Fe− and MnSOD activity decreases at high pH. However, studies on FeSOD revealed that K_M rather than k_{cat} changes as pH is increased, presumably due to competitive binding of OH^- to the oxidized protein at high pH.[2,3] While the same mode of inhibition (i.e., OH^- binding at high pH) was also invoked for Mn^{3+}SOD,[8] our data do not support this proposal (vide infra).

With the exception of a small number of so-called cambialistic SODs, most Fe− and MnSODs are strictly metal specific; i.e., neither Fe-substituted MnSODs, Fe-(Mn)SODs, nor Mn-substituted FeSODs, Mn(Fe)SODs, typically display catalytic activity.[1] Several factors have been proposed to contribute to this remarkable metal-ion specificity; e.g., enhanced anion affinity of Fe(Mn)-SOD, yielding a six-coordinate OH^- adduct at neutral pH;[9] distortions of the active site when the non-native metal is bound; and a mismatch in the reduction midpoint potential, E_m, of the metal-substituted SODs.[2,3] In support of the last proposal, redox titration experiments by Vance and Miller revealed that while the E_ms of the native SODs are almost identical and optimally tuned for $O_2^{\bullet-}$ disproportionation, Fe(Mn)SOD and Mn(Fe)SOD possess too low and too high a midpoint potential, respectively, for catalytic turnover (Figure 2).[2,3] Qualitatively, this result is

Timothy A. Jackson was born in Portage, WI, in 1978. He received his B.S. degree from St. Cloud State University (MN) in 2000 and is currently conducting research on superoxide dismutases in preparation of his Ph.D. thesis, under the supervision of Thomas C. Brunold.

Thomas C. Brunold was born in Bern, Switzerland, in 1969. He received his Ph.D. degree from the University of Bern in 1996, working with Hans U. Güdel on the design and spectroscopic characterization of new transition-metal-based near-IR laser materials. From 1997 to 1999 he was a postdoctoral fellow with Edward I. Solomon at Stanford University, studying binuclear iron and manganese centers in proteins and synthetic model complexes. He joined the faculty at the University of Wisconsin—Madison in 1999, where his research interests include spectroscopic and computational studies on superoxide dimsutases and Fe-, Co-, and Ni-containing enzymes and cofactors that form organometallic reaction intermediates.

* To whom correspondence should be addressed.

10.1021/ar030272h CCC: $27.50
Published on Web 05/19/2004

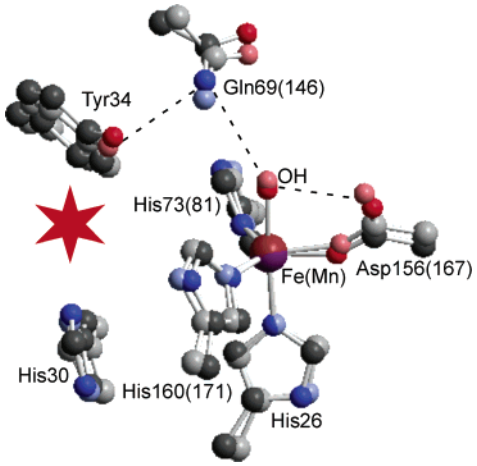

FIGURE 1. Overlay of active-site models of Fe^{3+}SOD (dark) and Mn^{3+}SOD (light) based on PDB files 1ISB and 1VEW, respectively. The numbering schemes relate to *E. coli* FeSOD and, in parentheses, MnSOD if different. The putative substrate prebinding site of FeSOD is indicated by an asterisk (*).

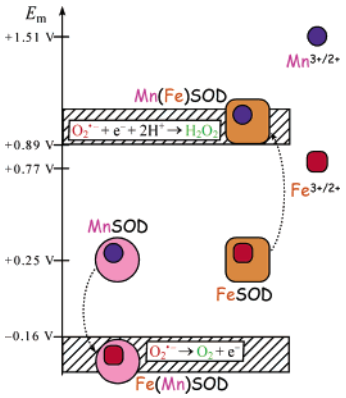

FIGURE 2. Reduction midpoint potentials (E_ms) of native and metal-substituted Fe− and MnSODs. Adapted from ref 2. Acceptable upper and lower limits for catalytic turnover are indicated. Note the vastly different E_ms of $Fe^{3+/2+}$ and $Mn^{3+/2+}$ in aqueous solution (far right).

understood by the considerably higher 3+/2+ redox potentials of Mn complexes relative to their Fe analogues, requiring MnSODs to depress the E_m of their active-site metal ion to a much greater extent than FeSODs (Figure 2). However, the geometric and electronic factors contributing to this difference in redox tuning are far from obvious, as the only notable difference between Fe− and MnSODs is the slightly different orientation of the second-sphere Gln69(146) (Figure 1), which derives from different subunits in the two proteins.

Spectroscopic/Computational Methodology

The combined spectroscopic/computational methodology employed in our research on Fe− and MnSODs is based largely on the pioneering work of Solomon and co-workers.[10] Table 1 provides an overview of the methods used in our laboratory and the insights they provide into geometric and electronic structure. Several recent developments have been crucial to the success of our research; e.g., the vast improvements in computer technology that now permit DFT calculations to be performed on realistic active-site models and the establishment of a theoretical framework by Neese and Solomon for the quantitative analysis of VTVH-MCD data for systems with spin $S > 1/2$ (Table 1).[11]

Metal Specificity

A notable feature of Fe− and MnSODs is that the protonation state of the coordinated solvent changes upon metal-ion oxidation/reduction (eq 2). As the extent to which protonation of this ligand is favored in each oxidation state will affect E_m, it was proposed that different H-bond interactions with the coordinated solvent may provide a mechanism by which Fe− and MnSODs differently tune the E_ms of their active-site metal ions.[2] To test this proposal, we used spectroscopic and computational techniques in conjunction with site-directed mutagenesis.[12]

Despite the fact that the metal-substituted enzyme is catalytically inactive, Abs, CD, and MCD data at pH 7 of FeSOD and Fe(Mn)SOD from *E. coli* (Figure 3) are remarkably similar, indicating that incorporation of Fe into (Mn)SOD preserves a five-coordinate, trigonal-bipyramidal active-site structure at physiological pH.[13] Thus, our spectroscopic data argue against models of SOD metal specificity invoking active-site distortions when the non-native metal is bound or direct modulation of the energy and/or nature of the metal 3d-based "redox-active" orbital.

Figure 4 shows active-site models obtained by partial DFT geometry optimizations for oxidized and reduced FeSOD (left) and derivatives thereof in which the second-sphere Gln and Tyr (modeled by acetamide and 4-methylphenol) were moved to their respective positions in MnSOD (right).[12] In the oxidized state, the decrease in distance between the Gln-derived NH_2 group and the oxygen of the OH^- ligand from 2.70 Å in Fe^{3+}SOD to 1.94 Å in the Fe^{3+}(Mn)SOD model leads to formation of a stronger H-bond and, thus, an increased stabilization of the ferric state in the metal-substituted enzyme. The relative stabilities are reversed in the reduced state, as proton uptake by the solvent ligand accompanying metal-ion reduction (eq 2) leads to considerably more steric interference between the Gln and H_2O protons in Fe^{2+}(Mn)SOD than in Fe^{2+}SOD (Figure 4, bottom). Hence, our calculations suggest that the closer proximity of the active-site Gln to the coordinated solvent in Fe(Mn)SOD than in FeSOD should result in a lower E_m, as observed experimentally (Figure 2). Despite these differences, DFT computations on the FeSOD and Fe(Mn)SOD models yield nearly identical molecular orbital (MO) descriptions, consistent with our spectroscopic data (Figure 3).

On the basis of our computations, replacement of the H-bond-donating Gln with an H-bond acceptor should greatly increase E_m by stabilizing Fe^{2+}-bound H_2O over Fe^{3+}-bound OH^-. This hypothesis was tested through construction of the Q69E FeSOD mutant in which Gln69 is replaced by an isosteric and isoelectronic Glu residue. Consistent with the conservative nature of this mutation,

Table 1. Overview of Spectroscopic and Computational Methods Employed in Our Fe− and MnSOD Research[a]

method	obtainable parameters	information content
	Ground State	
electron paramagnetic resonance (EPR)	*g* values; axial (*D*) and rhombic (*E*) zero-field splittings (ZFS)	spin of ground state; ligand-field (LF) splittings of metal 3d orbitals and their relative covalencies
	hyperfine couplings	spin distribution within molecule
variable-temperature/variable-field magnetic circular dichroism (VTVH MCD)	*g* values; ZFS parameters	see EPR above
	transition polarizations	identification of ligand(s) involved in charge-transfer (CT) transitions
resonance Raman (RR)	vibrational frequencies	force constants
	isotope shifts	band assignments; binding mode of exogenous ligands
	Excited States	
electronic absorption (Abs)	transition energies and intensities (oscillator strengths)	LF splittings of metal 3d orbitals; metal−ligand bond covalencies; relative energies of metal/ligand orbitals
	band shapes	excited-state distortions
circular dichroism (CD)	transition energies and intensities (rotational strengths)	same as Abs; resolution of overlapping bands in Abs spectrum, magnetic−dipole character of transition
magnetic CD (MCD)	transition energies and intensities (*A*, *B*, and *C* terms)	same as Abs; resolution of overlapping Abs bands, nature of excited states
	C/*D* ratio (∝MCD/Abs intensity)	metal character in transition
	Computations	
density functional theory (DFT)	energy-minimized metric parameters	structures and energies of hypothetical active-site models
	molecular orbital (MO) energies and compositions	quantitative bonding description
time-dependent (TD) DFT	predicted transition energies and Abs intensities	aids in evaluating hypothetical active-site models
INDO/S-CI	predicted spin Hamiltonian parameters (*g* values, *D*, and *E*) and transition energies and Abs intensities	same as TD-DFT

[a] See ref 10 for an excellent review of the spectroscopic methods typically employed in bioinorganic research.

MCD data for both the reduced and oxidized states of native and Q69E FeSOD are very similar, signifying that the Fe coordination environment is largely preserved in the mutant.[12] Nevertheless, Q69E FeSOD is completely inactive presumably due to the dramatically elevated E_m (by at least 600 mV).[14] Thus, replacement of Gln69 by Glu has the qualitative effect predicted by the computations, supporting our model that H-bonding interactions between Gln and coordinated solvent are intimately involved in the mechanism of E_m tuning employed by Fe− and MnSODs.

Active-Site p*K* Events

Kinetic and spectroscopic studies of Fe− and MnSODs led to the discovery of pH-dependent active-site transformations for both the reduced (p*K* values of 8.5 and 10.5, respectively)[2,3,15,16] and oxidized enzymes (p*K* ≈ 8.5 and 9.6, respectively).[2,3,8,16,17] Identifying the chemical event(s) associated with these p*K*s has been a major focus of SOD research, because active-site residues titrating near physiological pH may provide one of the two protons required for catalysis (eq 1; the other proton presumably stems from coordinated solvent). To explore the nature of these events, we characterized the neutral and high-pH forms of Fe− and MnSODs using our spectroscopic/computational methodology.[13]

Reduced Sites. Fe^{2+}SOD. NMR studies by Miller and co-workers revealed that the active-site p*K* of Fe^{2+}SOD is eliminated upon Y34F mutation, suggesting that deprotonation of Tyr34 is responsible for this p*K* event.[2,7] To test this hypothesis, near-IR CD and MCD spectra of Fe^{2+}-SOD were obtained at pH 7 and 11. Both data sets exhibit a weak LF transition at ∼10 500 cm^{-1}, indicating that the ferrous ion remains five-coordinate at high pH.[13] To complement these data, INDO/S-CI computations were performed on active-site models of Fe^{2+}SOD with the Tyr34 phenolic oxygen either protonated or deprotonated. These computations predict insignificant perturbations of the ground- and excited-state properties of the Fe^{2+} ion upon Tyr34 deprotonation, consistent with the minor spectroscopic changes associated with the active-site p*K* of ∼8.5. Thus, the active-site p*K* of Fe^{2+}SOD must be a second-sphere event that leaves the ferrous ion relatively unperturbed, compatible with (but not limited to) Tyr34 deprotonation.[13]

Oxidized Sites. Fe^{3+}SOD. The disappearance of the dominant Abs feature of *E. coli* Fe^{3+}SOD at ∼26 000 cm^{-1} (390 nm) at high pH was tentatively ascribed to OH^- binding to the ferric center on the basis of kinetic and spectroscopic studies of various Fe^{3+}SODs.[1,2] To elucidate the electronic origin of the spectroscopic changes at high pH, we first developed a rigorous assignment of the Abs spectrum of Fe^{3+}SOD at neutral pH (Figure 3). While the poor resolution of this spectrum precluded a detailed analysis, the combined use of Abs, CD, and MCD spectroscopies allowed us to determine the energies and oscillator strengths of the major Fe^{3+} d → d and LMCT transitions for this system (Table 2). To assist in our spectral analysis, INDO/S-CI computations were performed on the Fe^{3+}SOD active-site model in Figure 4. These computations suggest that the dominant Abs band at ∼26 000 cm^{-1} arises from an Asp156 → Fe^{3+} $3d_{x^2-y^2}$ CT

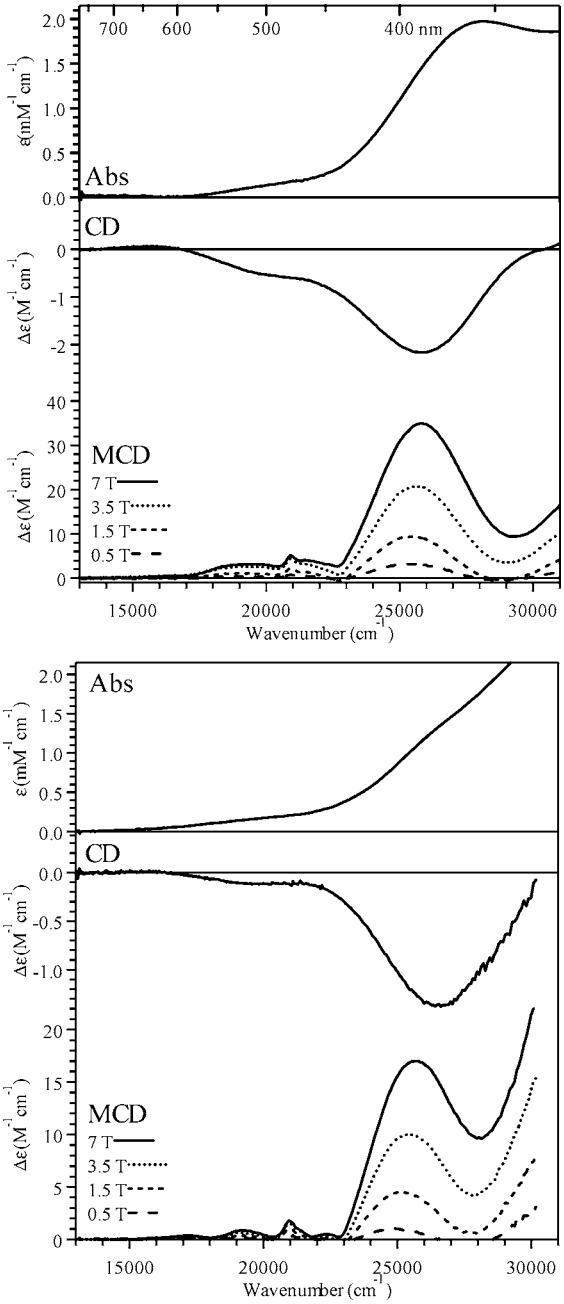

FIGURE 3. Abs, CD, and MCD spectra of Fe^{3+}SOD (top) and Fe^{3+}-(Mn)SOD (bottom) at 4.5 K and pH 7. Adapted from ref 13.

transition that is polarized along the *x*-axis of the **D**-tensor (i.e., roughly along the Fe−O(Asp156) axis, see Figure 5), consistent with our VTVH MCD data analysis for this feature. INDO/S-CI computations also properly predict several LF transitions in the visible/NIR spectral region (Table 2), indicating that this method is well suited for evaluating viable active-site models of high pH Fe^{3+}SOD on the basis of spectroscopic data.

Abs, CD, and MCD spectra of Fe^{3+} SOD at pH 10 reveal a blue shift in the Asp156 → Fe^{3+} $3d_{x^2-y^2}$ CT transition to >32 000 cm^{-1} and an apparent disappearance of the d → d transitions in the visible/NIR region (Table 2). As previous evidence suggested that OH^- binding to the Fe^{3+} center is responsible for these changes, we generated a hypothetical active-site model of high-pH Fe^{3+}SOD pos-

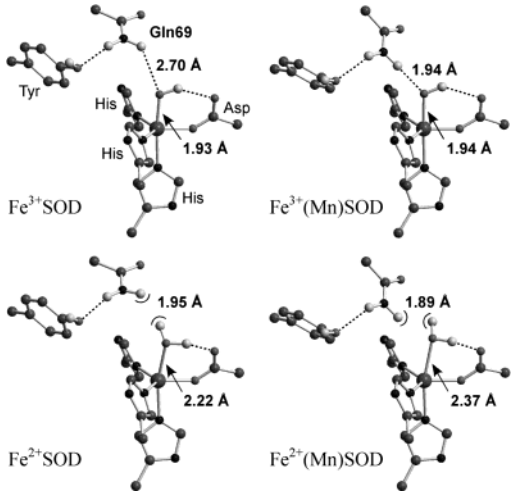

FIGURE 4. Active-site models for FeSOD (left) and Fe(Mn)SOD (right). For clarity, only protons involved in the active-site H-bond network are shown. Adapted from ref 12.

sessing an equatorial OH^- ion as a sixth ligand. INDO/S-CI computations for this OH−Fe^{3+}SOD model predict red-shifted d → d transitions and a blue shift of the Asp156 → Fe^{3+} $3d_{x^2-y^2}$ CT transition relative to Fe^{3+}SOD at pH 7 (Table 2). These changes can be rationalized by noting that OH^- binding (i) increases the effective ligand-field strength at the ferric center, thereby lowering the energies of the spin-forbidden d → d transitions observed experimentally, and (ii) considerably destabilizes the Fe $3d_{x^2-y^2}$-based MOs through a strong σ-antibonding interaction (Figure 5). Overall, the spectroscopic properties computed for OH−Fe^{3+}SOD are in excellent agreement with our experimental data of Fe^{3+}SOD at pH 10, providing additional evidence that the corresponding p*K* event involves OH^- binding to the ferric center at high pH.[13]

Mn^{3+}SOD. By analogy to Fe^{3+}SOD, observation that Mn^{3+}SOD exhibits a 20−30% loss of visible Abs intensity and a marked drop in catalytic activity with a p*K* of ∼9.7[8,17] was initially attributed to OH^- binding to the Mn^{3+} center at high pH. However, as mutations of Tyr34 and His30 eliminate the pH dependence of the Mn^{3+}SOD Abs spectrum while still allowing small anions to bind to the Mn^{3+} ion at neutral pH,[8,18] it was alternatively proposed that Tyr34 deprotonation might be responsible for this p*K*.[17] To discriminate between OH^- binding and Tyr34 deprotonation, we studied Mn^{3+}SOD at neutral and high pH.

MCD spectra of Mn^{3+}SOD at pH 7 and 11 (Figure 6, top and center) are remarkably similar, particularly in the visible/NIR region where the Mn^{3+} d → d transitions are observed. For comparison, MCD data were also collected for the azide adduct of Mn^{3+}SOD, a well-characterized six-coordinate Mn^{3+} species.[5] Importantly, the MCD spectrum of N_3−Mn^{3+}SOD (Figure 6, bottom) differs dramatically from those of Mn^{3+}SOD at neutral and high pH (Figure 6, top and center). Most notably, N_3−Mn^{3+}SOD exhibits a near-IR d → d transition (Figure 6, bottom inset) that is indicative of a six-coordinate Mn^{3+} center, consistent with X-ray data for this species.[5] Because spectroscopic data of Mn^{3+}SOD at pH 11 lack such a low-energy feature but

Table 2. Experimental Transitions Energies (cm^{-1}) and Oscillator Strengths for Fe^{3+}SOD at pH 7 and 11 and INDO/S-CI Computational Results for Our Fe^{3+}SOD and OH−Fe^{3+}SOD Models. Adapted from Ref 13

	pH 7 Fe^{3+}SOD (experimental)	Fe^{3+}SOD (INDO/S-CI)	pH 11 Fe^{3+}SOD (experimental)	OH−Fe^{3+}SOD (INDO/S-CI)
d → d[a]	<9 000	7 600		6 600
	10 800	8 600		6 800
		16 900		8 000
		17 400		9 900
	19 500 (f_{exp} = 0.002)	17 800		12 200
	21 500 (f_{exp} = 0.003)	21 000		13 000
		21 300		16 800
		22 600		22 000
Asp → Fe^{3+} LMCT		19 600 (f = 0.002)		31 500 (f = 0.001)
		20 000 (f = 0.002)		31 900 (f = 0.001)
		20 700 (f = 0.002)		32 000 (f = 0.003)
	26 000 (f_{exp} = 0.033)	21 100 (f = 0.063)		34 800 (f = 0.011)
		26 600 (f = 0.025)	>32 000 cm^{-1}	35 400 (f = 0.086)
D[b]	−1.7 cm^{-1}	−3.21 cm^{-1}	not determined	0.24 cm^{-1}
E/D[b]	0.24	0.17	not determined	0.20

[a] Calculated oscillator strengths for d → d transitions are 0 as our computations do not account for spin−orbit coupling among excited states. [b] Experimental ZFS parameters taken from ref 1.

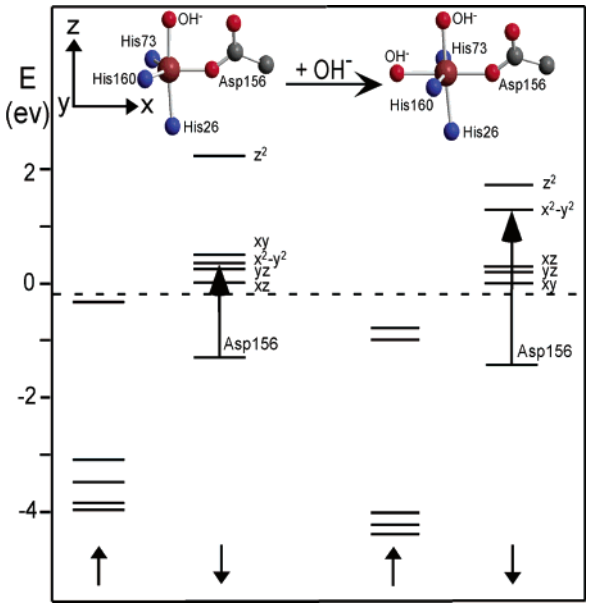

FIGURE 5. Relevant portions of MO diagrams for our Fe^{3+}SOD (left) and OH−Fe^{3+}SOD (right) models, obtained from spin-unrestricted DFT calculations. In each case the dominant Asp156 → Fe^{3+} $3d_{x^2-y^2}$ CT transition is indicated by an arrow. Adapted from ref 13.

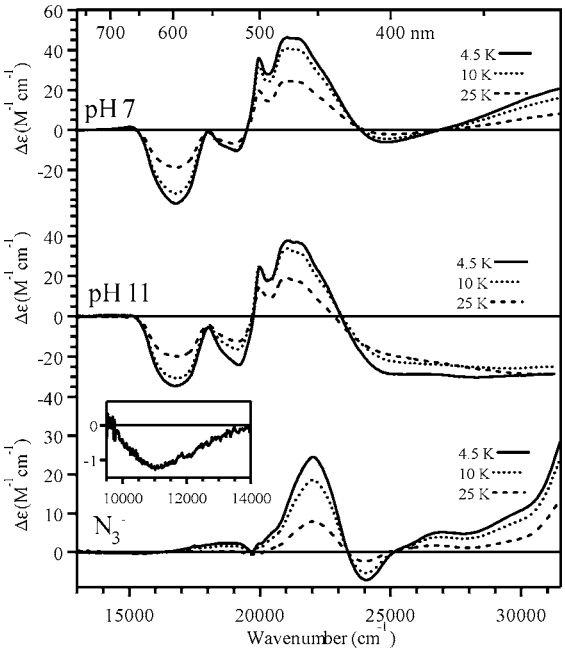

FIGURE 6. MCD spectra at 7 T of Mn^{3+}SOD at pH 7 (top) and 11 (center) and of N_3−Mn^{3+}SOD (bottom and inset). Adapted from ref 13.

instead highly resemble those obtained at neutral pH, the corresponding pK event does not appear to involve OH^- binding to the Mn^{3+} ion at high pH.

To complement our spectroscopic data, we employed DFT computations to generate active-site models for resting Mn^{3+}SOD and possible high pH forms (one six-coordinate model with an equatorial OH^- ligand, OH−Mn^{3+}SOD, and one five-coordinate with the phenolic oxygen of Tyr34 deprotonated, Mn^{3+}SOD($Y34^-$)). INDO/S-CI computations performed on our five-coordinate model of the resting state predict LF transition energies in excellent agreement with spectroscopic data obtained for Mn^{3+}SOD at pH 7. Analogous calculations on OH−Mn^{3+}SOD predict a dramatically altered spectrum in the visible region and the appearance of a LF transition at ∼9000 cm^{-1} (as observed for N_3−Mn^{3+}SOD, see Figure 6, bottom), in obvious disagreement with our high-pH data (Figure 6, center). In contrast, INDO/S-CI computations for Mn^{3+}SOD($Y34^-$) predict that deprotonation of Tyr34 leaves the energies of the LF transitions essentially unperturbed while slightly lowering their intensities. Thus, computations on this model nicely reproduce our spectroscopic data, strongly suggesting that Tyr34 deprotonation rather than OH^- binding to the Mn^{3+} center is responsible for the active-site pK of Mn^{3+}SOD.[13] Further support for this proposal comes from recent NMR experiments, which showed that the ^{13}C resonances associated with Tyr34 shift as pH is increased with a pK of ∼9.6.[16]

Collectively, our data suggest that the identity and oxidation state of the metal ion is integrally involved in determining the nature of the active-site pK event. However, this is not the only determining factor; rather, the protein matrix is also able to modulate the pK value and the relative stabilities of possible high-pH forms (e.g., first-

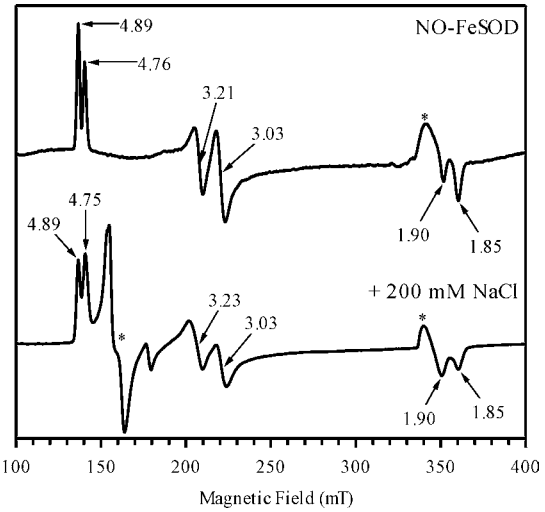

FIGURE 7. EPR spectra at 4 K of NO−FeSOD before (top) and after (bottom) incubation with 200 mM NaCl. Signals from free NO and nonspecifically bound Fe^{3+} are indicated by an asterisk (*). Adapted from ref 19.

sphere vs second-sphere events). For example, although the active-site Fe^{3+} ion is susceptible to OH^- binding, the (Fe)SOD protein matrix successfully prevents OH^- binding at physiological pH (p*K* of ∼9) while allowing substrate to freely access the Fe^{3+} center. Alternatively, the (Mn)-SOD protein matrix, which is optimally designed for Mn-supported activity, lacks such a discriminatory mechanism when Fe is bound, allowing partial OH^- binding to the ferric center even at neutral pH (p*K* of ∼6.4 for Fe^{3+}(Mn)-SOD).[2,8]

Active-Site/Substrate Analogue Interactions

As the catalytic rates of Fe− and MnSODs approach the diffusion-controlled limit, it is practically impossible to trap true reaction intermediates. To obtain clues as to whether catalysis proceeds through formation of inner-sphere or outer-sphere complexes, substrate analogues have therefore been used extensively to model active-site/substrate interactions.[1] Our research has aimed at generating geometric and electronic structure descriptions of these metal-ion adducts, especially in cases where X-ray studies were unsuccessful or hampered by the presence of multiple species.

Reduced Sites. Fe^{2+}SOD. While previous studies revealed that NO binds to the active-site ferrous ion of Fe^{2+}-SOD to generate an {Fe−NO}^{7} system,[15] this species exhibits two $S = 3/2$ EPR signals (Figure 7, top).[15,19] Our simulation of these data reveals that the two $S = 3/2$ signals have comparable populations (42% and 58%) and rather large rhombicities ($E/D = 0.128$ and 0.154, respectively[19]) compared to typical {Fe−NO}^{7} systems, reflecting somewhat unusual ground-state properties of NO−Fe-SOD. The 300 K Abs spectrum of NO−FeSOD (Figure 8, top) shows the three-band pattern characteristic of six-coordinate {Fe−NO}^{7} species, indicating that NO binding to Fe^{2+}SOD leads to an expansion of the coordination sphere of the Fe center. From an iterative Gaussian deconvolution of Abs and MCD spectra of NO−FeSOD,

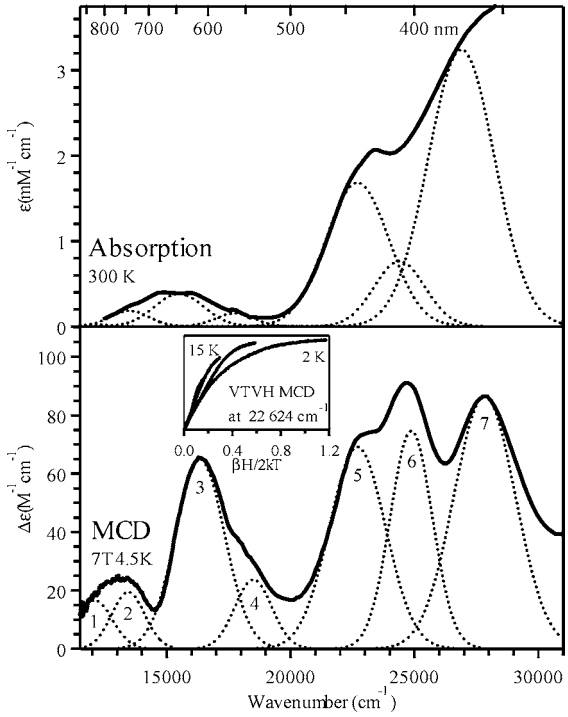

FIGURE 8. Abs (top) and MCD data (bottom and inset) of NO−FeSOD. The results from a Gaussian deconvolution of these spectra are shown by dotted lines. Adapted from ref 19.

seven electronic transitions could be resolved (Figure 8), of which three (bands 3, 5, and 7) correspond to $NO^- \rightarrow Fe^{3+}$ CT transitions and the remaining four to formally spin-forbidden Fe^{3+} d → d transitions. VTVH MCD data collected for the $NO^- \rightarrow Fe^{3+}$ CT transitions (Figure 8, bottom inset) were successfully fit using either set of experimentally determined ZFS parameters (i.e., $E/D =$ 0.154 or 0.128), in each case predicting the transitions to be predominantly *z*-polarized (∼80%) with a minor *y*-component (∼20%). Interestingly, our Abs and MCD data of NO−FeSOD appear consistent with the presence of a single {Fe−NO}^{7} species, as opposed to two required by EPR data.

In an effort to rationalize these findings, we employed DFT and INDO/S-CI calculations. An important issue that needed to be addressed in these computations concerned the protonation state of the axial solvent ligand. While NO binding to Fe^{2+}SOD (possessing an axial H_2O ligand) formally oxidizes the ferrous center by one electron, thus generating a ferric site that may be expected to coordinate OH^-, the high covalency of the Fe−NO bond leads to significant electron delocalization from the NO^- ligand onto the Fe^{3+} ion. To resolve this ambiguity, we performed full DFT geometry optimizations on NO−FeSOD active-site models possessing either an axial OH^- or H_2O ligand (NO−$FeSOD^{OH}$ and NO−$FeSOD^{H2O}$, respectively) and evaluated these models on the basis of our experimental data. As summarized in Table 3, the presence of an axial OH^- ligand is required to properly reproduce both the high rhombicity and the large splitting of the two lower-energy $NO^- \rightarrow Fe^{3+}$ CT transitions observed experimentally, indicating that the solvent ligand releases a proton

Table 3. Relative Total Energies (kcal/mol), CT Transitions Energies (cm^{-1}), and ZFS Parameters for NO−FeSOD Models. Adapted from Ref 19

	relative energy	D (cm^{-1})	E/D	NO π_{ip}^* → Fe $3d_{yz}$	NO π_{op}^* → Fe $3d_{xz}$	NO π_{ip}^* → Fe $3d_{z^2}$
experimental		6 ± 1	0.154 and 0.128	15 500	22 700	26 900
Fe−N−O angle[a]						
140°	1.499	1.46	0.209	15 700	20 500	26 900
145°	0	1.57	0.179	13 400	20 600	26 600
150°	1.694	1.79	0.149	14 600	20 700	26 200
O_{sol}−Fe−N−O angle[a]						
10°	1.316	1.64	0.113	13 400	20 600	26 600
20°	0	1.57	0.179	13 400	20 600	26 600
30°	1.597	1.66	0.152	13 500	20 500	26 600
NO−FeSOD^{H2O}		1.54	0.018	15 500	18 600	26 700

[a] Calculations performed on NO−FeSOD^{OH} models possessing an axial OH^- ligand.

when NO binds to Fe^{2+}SOD.[19] Considering that NO binding to Fe^{2+}SOD thus adequately mimics key steps in the reductive half-reaction of the catalytic cycle (eq 1b), involving oxidation of Fe^{2+} to Fe^{3+} and deprotonation of the axial solvent ligand, it is tempting to speculate that the reaction of Fe^{2+}SOD with the actual substrate also proceeds through formation of an inner-sphere complex.

Starting from our experimentally validated NO−FeSOD model, we performed additional computations to explore if conformational variations in the {Fe−NO}^{7} unit could be responsible for the two slightly different species observed by EPR spectroscopy. These computations reveal that a small change in the Fe−N−O angle and/or rotation about the Fe−NO bond alter the rhombicity of the system without appreciably changing the $NO^- \rightarrow Fe^{3+}$ CT transition energies (Table 3). Importantly, both of these distortions from the equilibrium geometry come at a low energetic cost (∼1.5 kcal/mol), suggesting that in NO−FeSOD two nearly isoenergetic conformations of the {Fe−NO}^{7} unit exist that give rise to slightly different $S = 3/2$ EPR signals but virtually identical Abs and MCD spectra. In support of this proposal, we showed that the relative intensities of the two $S = 3/2$ signals can be modulated by incubating NO−FeSOD with excess Cl^- (Figure 7, bottom), which presumably leads to partial occupancy of the substrate prebinding site located near Tyr34 (Figure 1).[19] Intriguingly, as a water molecule occupies the prebinding site in resting FeSOD, this result along with the fact that Tyr34 titrates near physiological pH (vide supra) may also support the notion that a proton relay involving Tyr34 and His30 exists that ensures rapid proton delivery from bulk water to coordinated substrate during catalysis (eq 1).

Oxidized Sites. Fe^{3+}SOD. Fe^{3+}SOD was shown to bind a number of small anions, among which azide received particular interest due to its substrate-like charge and frontier orbitals. Crystallographic studies revealed that azide binding to Fe^{3+}SOD yields a six-coordinate complex (Figure 9, inset).[5] Interestingly, two distinct complexes can be generated upon freezing of N_3−Fe^{3+}SOD solutions: a pink species (at low protein concentrations and $[N_3^-]/[Fe^{3+}SOD] > 2$) and a yellow species (in all other instances), which were tentatively described as six-coordinate Fe−N_3 complexes with two and one azide ligand(s), respectively.[20] As Fe^{3+}SOD's ability to bind two azide molecules could have important implications with respect

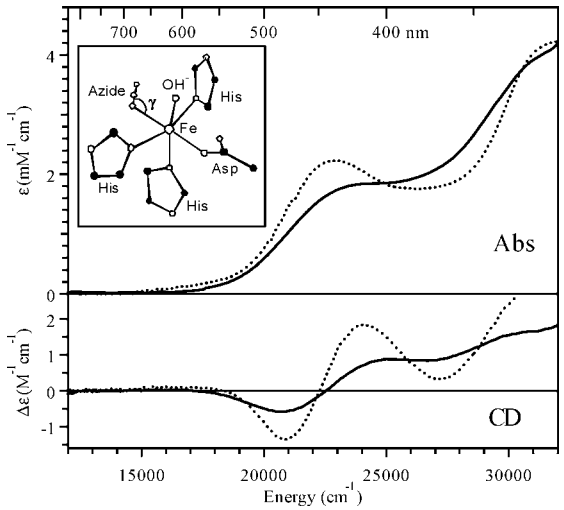

FIGURE 9. Abs and CD spectra at 300 (solid lines) and 4.5 K (dotted lines) of the yellow N_3−Fe^{3+}SOD adduct. Adapted from ref 21. (Inset) Active site of N_3−Fe^{3+}SOD based on PDB file 1ISC.

to the catalytic mechanism, we performed a detailed characterization of the yellow and pink N_3−Fe^{3+}SOD complexes.[21]

Figure 9 shows Abs and CD spectra of the yellow N_3−Fe^{3+}SOD adduct at 4.5 and 300 K. Aside from the expected band sharpening with decreasing temperature, the two data sets are nearly identical, both exhibiting a prominent Abs feature at ∼22 500 cm^{-1} that was previously assigned as an $N_3^- \rightarrow Fe^{3+}$ CT transition. While the 300 K data of N_3−Fe^{3+}SOD samples that turn pink upon freezing are identical to those in Figure 9, the red shift of the Abs envelope at 4.5 K indicates formation of a different species at low temperature. However, MCD data of the yellow and pink N_3−Fe^{3+}SOD complexes (Figure 10) are in fact quite similar, the only difference being the energy of the dominant $N_3^- \rightarrow Fe^{3+}$ CT band. Such similarities suggest that both species actually possess a single azide ligand.

To explore whether second-sphere perturbations might be responsible for the spectral differences between yellow and pink N_3−Fe^{3+}SOD, we also characterized the azide complex of Q69E Fe^{3+}SOD. Despite the lack of a direct interaction between Gln69 and the azide ligand in the native complex, the dominant $N_3^- \rightarrow Fe^{3+}$ CT transition of Q69E N_3−Fe^{3+}SOD is downshifted by more than 2000 cm^{-1}, yielding a red species at all temperatures.

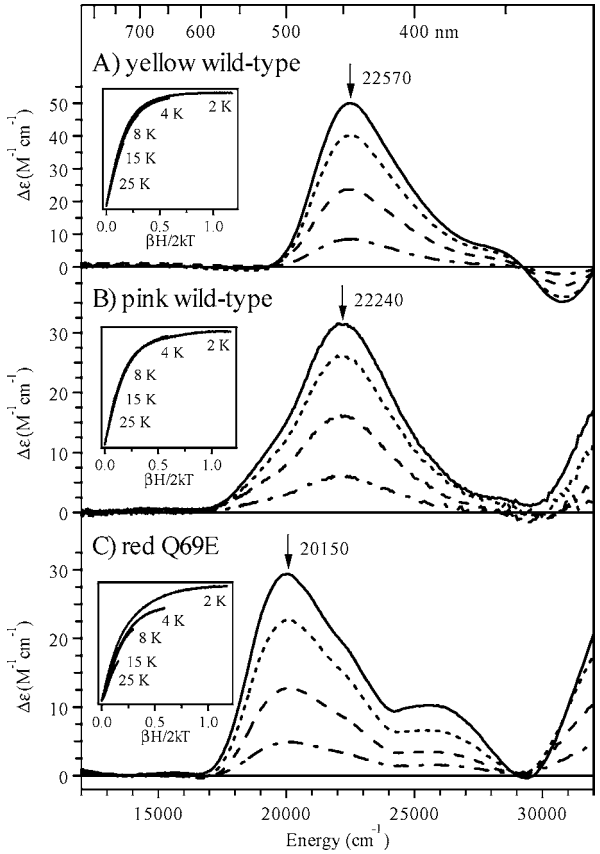

FIGURE 10. Variable-field (0.5, 1.5, 3.5, and 7 T) MCD spectra at 4.5 K of the yellow (A) and pink (B) wild-type and the Q69E (C) N_3−Fe^{3+}SOD adducts. Adapted from ref 21. (Insets) VTVH MCD data obtained at the positions indicated by arrows.

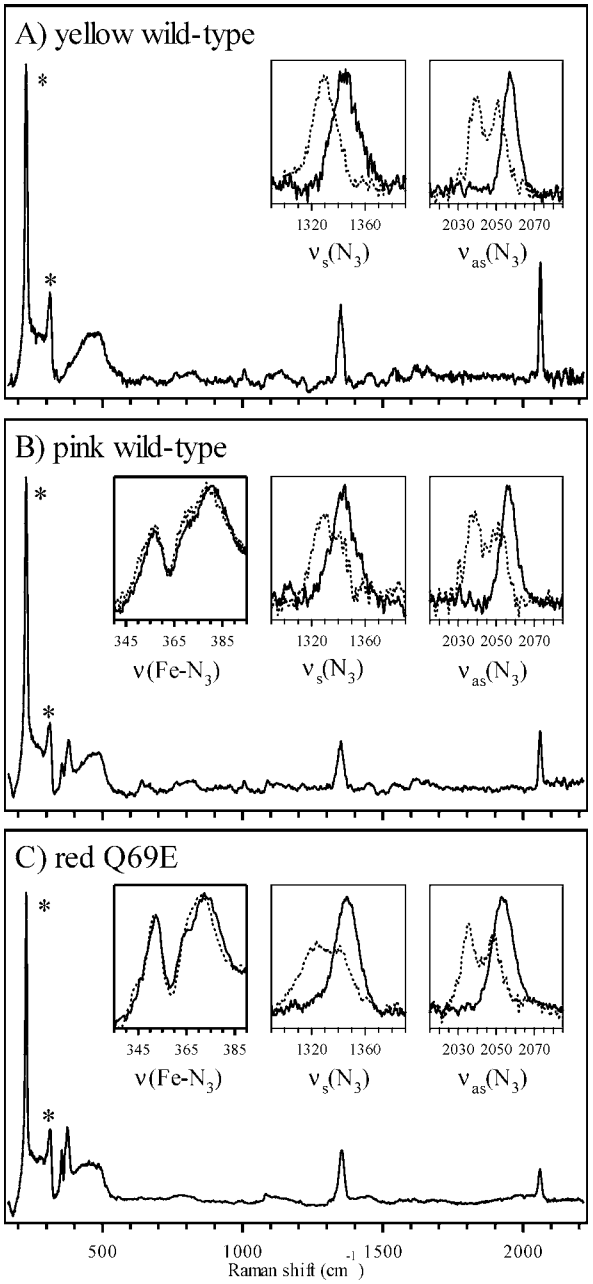

FIGURE 11. RR spectra at 77 K of the yellow (A) and pink (B) wild-type and the Q69E (C) N_3−Fe^{3+}SOD adducts for 515 nm excitation. Adapted from ref 21. Ice peaks are indicated by an asterisk (*). (Insets) Expanded views of the protein-derived features for samples prepared with $^{14}N_3$ (solid lines) and ^{15}N−$^{14}N_2$ (dotted lines).

The three N_3−Fe^{3+}SOD adducts were further studied using RR spectroscopy. In RR spectra obtained with 515 nm excitation (Figure 11), protein-derived features are discernible at ∼370 (a group of three closely spaced bands), 1350, and 2050 cm^{-1}. RR data obtained on samples prepared with terminally ^{15}N-labeled azide exhibit downshifts and splittings of the two higher energy bands and reveal that the highest energy component of the ∼370 cm^{-1} feature is also isotope sensitive (Figure 11, insets). From a normal coordinate analysis of the Fe−N_3 unit, the three isotope-sensitive bands correspond to the Fe−N_3 stretch and the symmetric and antisymmetric intra-azide stretches (in order of increasing energy). Thus, our RR experiments also indicate that a single azide ligand is present in all three N_3−Fe^{3+}SOD complexes investigated.

A clue as to possible differences between these N_3−Fe^{3+}SOD complexes comes from the crystal structures of N_3−Fe^{3+}SOD and N_3−Mn^{3+}SOD, which reveal considerably different metal−N−N bond angles of $\gamma = 117°$ and 147°, respectively. An increase in γ would be expected to reduce the σ-bonding interaction between Fe^{3+} and the azide π^{nb} orbital oriented in the Fe−N_3 plane and, thus, to lower the energy E_{CT} of the corresponding $N_3^- \rightarrow Fe^{3+}$ CT transition. To establish a quantitative correlation between γ and E_{CT}, we performed INDO/S-CI calculations on a series of N_3−Fe^{3+}SOD active-site models with different values of γ. For $\gamma = 120°$, INDO/S-CI computations predict a single intense $N_3^- \rightarrow Fe^{3+}$ CT transition at 20 930 cm^{-1}, in good agreement with $E_{CT} \approx 22\,500$ cm^{-1} for the yellow N_3−Fe^{3+}SOD adduct where $\gamma = 117°$ (Figure 9). With increasing γ, E_{CT} shifts to 20 520 cm^{-1} (130°), 19 740 cm^{-1} (140°), and 18 330 cm^{-1} (150°), supporting our hypothesis that variations in γ modulate the color of N_3−Fe^{3+}SOD species.

Collectively, our data provide strong evidence that both the yellow and pink N_3−Fe^{3+}SOD complexes possess a single azide ligand but differ with respect to γ by ∼10°.[21] Formation of the pink species only when $[N_3^-]/[Fe^{3+}SOD] > 2$ may reflect a necessity for binding of an additional N_3^- molecule to the putative prebinding site near Tyr34

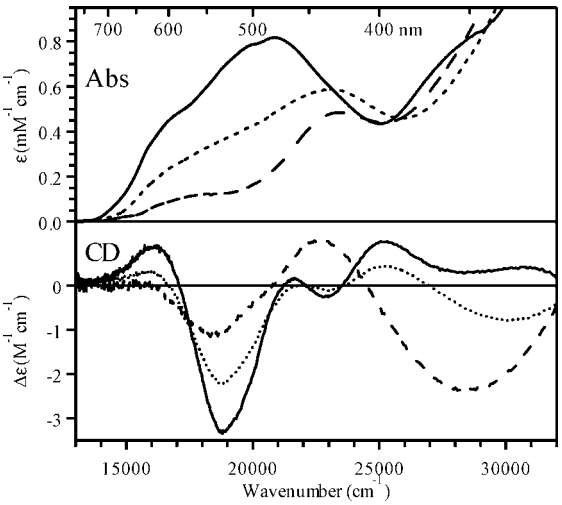

FIGURE 12. Abs and CD spectra at 300 K of resting Mn^{3+}SOD (solid line), RT N_3−Mn^{3+}SOD (dotted line), and Y34F N_3−Mn^{3+}SOD (dashed line; a model of six-coordinate LT N_3−Mn^{3+}SOD).

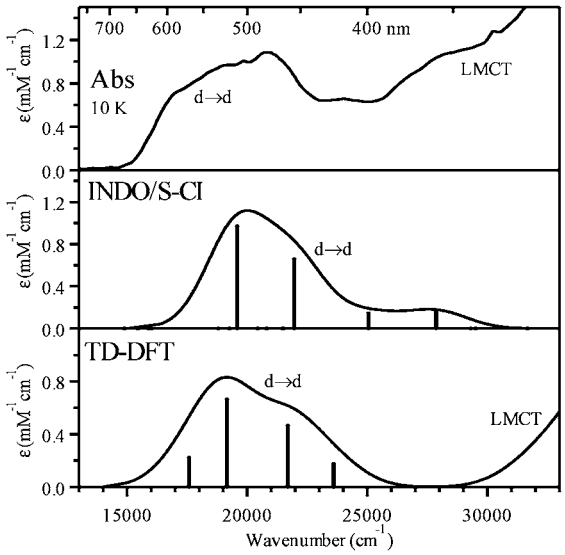

FIGURE 13. Experimental Abs spectrum of Mn^{3+}SOD (top) and simulated spectra based on INDO/S-CI (center) and TD-DFT (bottom) computations for our Mn^{3+}SOD active-site model.

(Figure 1). Steric and electrostatic changes associated with N_3^- incorporation into this prebinding site could be propagated through the H-bond network including Tyr34, Gln69, and coordinated solvent to perturb Fe−N_3 bonding interactions. Support for this model is provided by the altered color of the Q69E N_3−Fe^{3+}SOD species in which this H-bond network is perturbed. These findings suggest that second-sphere residues may play an important role in orienting incoming substrate for reaction with the FeSOD active site. Notably, the strongest Fe−N_3 σ-bonding interaction is calculated for $\gamma = 120°$, close to $\gamma = 117°$ observed for N_3−FeSOD at physiological temperature. By orienting the substrate molecule in a similar way, the second coordination sphere could ensure large electronic coupling between $O_2^{\bullet-}$ and Fe^{3+}, thereby reducing the Franck−Condon barrier to electron transfer.

Mn^{3+}SOD. Variable-temperature Abs and CD studies revealed that the N_3−Mn^{3+}SOD complexes from *E. coli* and *T. thermophilus* are thermochromic, exhibiting distinct spectral features above and below an organism-dependent transition temperature (225 and 305 K, respectively).[22] Spectroscopic and X-ray data indicated that the active site of the low-temperature (LT) form of N_3−Mn^{3+}-SOD is six-coordinate, with azide occupying the open coordination site of the resting enzyme (Figure 1).[5] Alternatively, Abs and CD spectra of the room-temperature (RT) form are characteristic of a five-coordinate Mn^{3+} center based on the absence of a LF band in the NIR region;[22] however, the identity of the ligand that dissociates upon conversion of LT to RT N_3−Mn^{3+}SOD remained unknown.

Our Abs and CD spectra of resting Mn^{3+}SOD and the LT and RT forms of N_3−Mn^{3+}SOD reveal that the LF transition energies of the Mn^{3+} ion are hardly affected by the addition of azide to Mn^{3+}SOD at RT but change drastically upon conversion to LT N_3−Mn^{3+}SOD (Figure 12). Quantitative analysis of these spectra indicates that Mn^{3+}SOD and RT N_3−Mn^{3+}SOD also exhibit similarly intense near-UV CT transitions, thus arguing against the appearance of intense $N_3^- \rightarrow Mn^{3+}$ CT transitions upon incubation of Mn^{3+}SOD with azide. This result, along with the insignificant effects of azide on the LF transitions and, hence, the coordination environment of the active-site Mn^{3+} ion, suggest that azide does not actually coordinate to the Mn^{3+} ion at RT.

To unambiguously assess whether dissociation of coordinated solvent, Asp167, or azide is responsible for the thermochromism of N_3−Mn^{3+}SOD, several hypothetical five-coordinate active-site models were derived from the X-ray structure of six-coordinate N_3−Mn^{3+}SOD.[23] Four models were generated by increasing either the Mn−O(solvent) or Mn−O(Aps167) bond length to 2.4 Å for both OH^- and H_2O as possible solvent protonation states, and one model was obtained by placing the azide molecule within H-bonding distance of the phenolic oxygen of Tyr34 and remote from the Mn^{3+} ion (Mn−N(N_2) distance of 3.5 Å). Constrained DFT geometry optimizations of these models, in which the positions of the H_3C_β groups of the first-sphere residues and all atoms of second-sphere residues not involved in the H-bond network (Figure 1) were held fixed, revealed that only geometry optimization of the model used to explore N_3^- dissociation (N_3−Mn^{3+}-SOD^{OH}[−N_3]) yielded a five-coordinate Mn^{3+} ion. Importantly, the calculated total energy of this model is only 6.2 kcal/mol higher than that of our six-coordinate model of LT N_3−Mn^{3+}SOD, consistent with the experimental enthalpy difference of ∼5 kcal/mol between the LT and RT forms.[22]

To assess whether the N_3−$Mn^{3+}$$SOD^{OH}$[−$N_3$] model would also be consistent with our spectroscopic data of RT N_3−Mn^{3+}SOD, we calculated the corresponding Abs spectrum using time-dependent (TD) DFT computations. This method was used instead of the INDO/S-CI method as parallel studies using Mn^{3+}SOD and LT N_3−Mn^{3+}SOD as well-characterized reference systems revealed that the latter method accurately predicts Mn^{3+} d → d transition

energies but consistently overestimates LMCT transition energies whereas the TD-DFT method predicts both Mn^{3+} d → d and LMCT transition energies in good agreement with experimental data (Figure 13). The TD-DFT-computed Abs spectrum for $N_3{-}Mn^{3+}SOD^{OH}[{-}N_3]$ is consistent with our experimental RT $N_3{-}Mn^{3+}SOD$ Abs spectrum, strongly suggesting that (entropy-driven) dissociation of azide causes the thermochromic behavior of $N_3{-}Mn^{3+}$-SOD.[23] Importantly, this model also explains why Y34F $Mn^{3+}SOD$, which lacks this outer-sphere binding site for azide, forms a six-coordinate $Mn{-}N_3$ adduct at all temperatures.[8]

Concluding Remarks

Through the use of a combined spectroscopic/computational methodology, we demonstrated that second-sphere residues are critically involved in controlling both thermodynamic and kinetic properties of the Fe− and MnSOD active sites. Specifically, results presented in this Account demonstrate that (i) Gln69(146) (Figure 1) plays a crucial role in optimally tuning the active-site E_m for $O_2^{\bullet-}$ disproportionation[12] while also preventing dissociation of coordinated solvent upon binding of substrate (analogues), possibly avoiding the detrimental formation of long-lived reaction intermediates such as side-on bound peroxo species[19] (note that other non-heme iron enzymes bind NO by dissociating coordinated solvent); (ii) Tyr34 likely provides one of the two protons required for catalysis, thereby facilitating product release and contributing to the fast turnover rate;[13,16] and (iii) the ensemble of several second-sphere residues that are intimately coupled through an elaborate H-bond network likely aid in discriminating between substrate and OH^- at physiological pH, orienting incoming substrate for rapid electron transfer with the active-site metal ion, and determining the relative stabilities of viable active-site/substrate analogue complexes.[13,19,21] In the future we plan to extend our research on Fe− and MnSODs to include the design and characterization of additional mutants possessing novel properties and altered reactivities and to augment our arsenal of spectroscopic and computational tools with QM/MM calculations, which should sharpen our molecular-level understanding of the mechanisms by which second-sphere residues tune the active-site properties of these fascinating enzymes.

This research has been supported by the NIH (GM 64631) and the University of Wisconsin Biophysics Training Grant (fellowship to T.A.J). The authors thank Dr. Juan Xie whose hard work is also covered in this Account, Professor Anne-Frances Miller and her students for their generous protein supply and invaluable discussions, and Dr. Frank Neese for his contributions to the computational aspects of this research.

References

(1) Miller, A.-F.; Sorkin, D. L. Superoxide Dismutases: A Molecular Perspective. *Comments Mol. Cell. Biophys.* **1997**, *9*, 1−48 and references therein.
(2) Miller, A.-F. In *Handbook of Metalloproteins*; Messerschmidt, A., Huber, R., Poulos, T., Wieghardt, K., Eds.; John Wiley & Sons: Chichester, 2001; pp 668−682 and references therein.
(3) Miller, A.-F. In *Comprehensive Coordination Chemistry II*; McCleverty, J. A., Meyer, T. J., Eds.; Elsevier Ltd.: Oxford, U.K., 2004; Vol. 8, pp 479−506 and references therein.
(4) *Methods in Enzymology: Superoxide Dismutase*; Packer, L., Ed.; Academic Press: San Diego, 2002; Vol. 349, pp 400 and references therein.
(5) Lah, M. S.; Dixon, M. M.; Pattridge, K. A.; Stallings, W. C.; Fee, J. A.; Ludwig, M. L. Structure−Function in *Escherichia coli* Iron Superoxide Dismutase: Comparisons with the Manganese Enzyme from *Thermus thermophilus*. *Biochemistry* **1995**, *34*, 1646−1660.
(6) Edwards, R. A.; Baker, H. M.; Whittaker, M. M.; Whittaker, J. W.; Jameson, G. B.; Baker, E. N. Crystal Structure of *Escherichia coli* Manganese Superoxide Dismutase at 2.1-Å Resolution. *J. Biol. Inorg. Chem.* **1998**, *3*, 161−171.
(7) Miller, A.-F.; Padmakumar, F.; Sorkin, D.; Karapetian, A.; Vance, C. K. Proton-coupled electron transfer in Fe-superoxide dismutase and Mn-superoxide dismutase. *J. Inorg. Biochem.* **2003**, *93*, 71−83.
(8) Whittaker, M. M.; Whittaker, J. W. Mutagenesis of a Proton Linkage Pathway in *Escherichia coli* Manganese Superoxide Dismutase. *Biochemistry* **1997**, *36*, 8923−8931.
(9) Edwards, R. A.; Whittaker, M. M.; Whittaker, J. W.; Jameson, G. B.; Baker, E. N. Distinct Metal Environment in Fe-Substituted Manganese Superoxide Dismutase Provides a Structural Basis of Metal Specificity. *J. Am. Chem. Soc.* **1998**, *120*, 9684−9685.
(10) Solomon, E. I.; Hanson, M. A. In *Inorganic Electronic Structure and Spectroscopy*; Solomon, E. I., Lever, A. B. P., Eds.; Wiley: New York, 1999; Vol. 2, pp 1−130.
(11) Neese, F.; Solomon, E. I. MCD C-term Signs, Saturation Behavior, and Determination of Band Polarizations in Randomly Oriented Systems with Spin $S \geq 1/2$. Application to $S = 1/2$ and $S = 5/2$. *Inorg. Chem.* **1999**, *38*, 1847−1865.
(12) Yikilmaz, E.; Xie, J.; Brunold, T. C.; Miller, A.-F. Hydrogen-Bond Mediated Tuning of the Redox Potential of the Non-Heme Fe Site of Superoxide Dismutase. *J. Am. Chem. Soc.* **2002**, *124*, 3482−3483.
(13) Jackson, T. A.; Xie, J.; Yikilmaz, E.; Miller, A.-F.; Brunold, T. C. Spectroscopic and Computational Studies on Iron and Manganese Superoxide Dismutases: Nature of the Chemical Events Associated with Active Site p*K*s. *J. Am. Chem. Soc.* **2002**, *124*, 10833−10845.
(14) Yikilmaz, E.; Miller, A.-F. Manuscript in preparation.
(15) Niederhoffer, E. C.; Fee, J. A.; Papaefthymiou, V.; Münck, E. Magnetic Resonance Studies Involving Iron Superoxide Dismutase from *Escherichia coli*. In *Isotope and Nuclear Chemistry Division Annual Report*; Los Alamos National Laboratory: Los Alamos, 1987.
(16) Maliekal, J.; Karapetian, A.; Vance, C.; Yikilmaz, E.; Wu, Q.; Jackson, T.; Brunold, T. C.; Spiro, T. G.; Miller, A.-F. Comparison and Contrasts between the Active Site p*K*s of Mn−Superoxide Dismutase and Those of Fe−Superoxide Dismutase. *J. Am. Chem. Soc.* **2002**, *124*, 15064−15075.
(17) Hsu, J. L.; Hsieh, Y. S.; Tu, C. K.; O'Connor, D.; Nick, H. S.; Silverman, D. N. Catalytic Properties of Human Manganese Superoxide Dismutase. *J. Biol. Chem.* **1996**, *271*, 17687−17691.
(18) Edwards, R. A.; Whittaker, M. M.; Whittaker, J. W.; Baker, E. N.; Jameson, G. B. Outer Sphere Mutations Perturb Metal Reactivity in Manganese Superoxide Dismutase. *Biochemistry* **2001**, *40*, 15−27.
(19) Jackson, T. A.; Yikilmaz, E.; Miller, A.-F.; Brunold, T. C. Spectroscopic and Computational Study of a Non-Heme Iron $\{Fe{-}NO\}^7$ System: Exploring the Geometric and Electronic Structures of the Nitrosyl Adduct of Iron Superoxide Dismutase. *J. Am. Chem. Soc.* **2003**, *125*, 8348−8363.
(20) Slykhouse, T. O.; Fee, J. A. Physical and Chemical Studies on Bacterial Superoxide Dismutases. *J. Biol. Chem.* **1976**, *251*, 5472−5477.
(21) Xie, J.; Yikilmaz, E.; Miller, A.-F.; Brunold, T. Second-Sphere Contributions to Substrate-Analog Binding in Iron(III) Superoxide Dismutase. *J. Am. Chem. Soc.* **2002**, *124*, 3769−3774.
(22) Whittaker, M. M.; Whittaker, J. W. A "Thermophilic Shift" in Ligand Interactions for *Thermus thermophilus* Manganese Superoxide Dismutase. *J. Biol. Inorg. Chem.* **1997**, *2*, 667−671.
(23) Jackson, T. A.; Brunold, T. C. Manuscript in preparation.

AR030272H